value from torque-sharing controller

demanded by the controller

passed through clutch

scaled by gearbox

motor

rotor

turboshaft

# GT2021-59375

# REVOLUTIONARY VERTICAL LIFT TECHNOLOGY (RVLT) SIDE-BY-SIDE HYBRID CONCEPT VEHICLE POWERTRAIN DYNAMIC MODEL

	Santino J. Bianco NASA John H. Glenn Research Center Cleveland, OH	Christine T. Chevalier HX5, LLC Brook Park, OH	Jonathan S. Litt NASA John H. Glenn Research Center Cleveland, OH	Joshua K. Smith (Intern) NASA John H. Glenn Research Center Cleveland, OH	Jeffryes W. Chapman NASA John H. Glenn Research Center Cleveland, OH	Jonathan L. Kratz NASA John H. Glenn Research Center Cleveland, OH	
ABSTRACT  The Side-by-Side (SBS) Hybrid is one of several Revolutionary Vertical Lift Technology (RVLT) concept aircraft identified by NASA to investigate Urban Air Mobility (UAM) requirements. This paper presents a dynamic model of the SBS Hybrid powertrain built using the Toolbox for the Modeling and Analysis of Thermodynamic Systems (T-MATS) and the Electrical Modeling and Thermal Analysis Toolbox (EMTAT). The model consists of the rotors, electrical power system, and turboshaft engines connected through freewheeling clutches, gearboxes, and multiple shafts. This research effort models the complex behavior of the powertrain, including the operation of the freewheeling clutches and electrical power system at the simulation time scale of the shaft dynamics. Several simulations highlight the key features present in the model and demonstrate its operation.  Keywords: revolutionary vertical lift technology, side-byside hybrid concept, powertrain, dynamic model, electrified aircraft propulsion				$K_I$ $K_P$ $K_T$ $\min$ () $MN$ $n$ $N$ $\dot{N}$ $NASA$ NDARC $NPSS$ $PI$ $pps$ $RVLT$ $SBS$ $T$ $T-MATS$	integral gain proportional gain torque-sharing controller gain minimum value of arguments Mach number gear ratio shaft speed shaft acceleration National Aeronautics and Space Administration NASA Design and Analysis of Rotorcraft Numerical Propulsion System Simulation proportional-integral pounds per second Revolutionary Vertical Lift Technology side-by-side torque Toolbox for the Modeling and Analysis of Thermodynamic Systems		
NOMEN AGL Alt				UAM WATE++ <i>Wf</i> η	Urban Air Mobility Weight Analysis of Turbine Engines fuel flow rate gearbox efficiency		
b CP dT e EAP	angular vis collective p temperatur speed error	e difference from	•	Subscripts  A  cmd  cmd + bias	augmented by the commanded by the power turbine spe	e gearbox	

EM

fpm

**IWP** 

 $K_{aw}$ 

J

**EMTAT** 

electric machine

feet per minute

integral windup protection

angular moment of inertia

integral windup protection gain

Toolbox

Electrical Modeling and Thermal Analysis

1 This material is declared a work of the U.S. Government and is not subject to copyright protection in the United States. Approved for public release; distribution is unlimited.

dmd

Μ

T

R

P

S

- x shaft number
- y freewheeling clutch number

### 1. INTRODUCTION

In the near future, it is expected that electrified aircraft propulsion (EAP) will be used in several new types of vertical lift vehicles for Urban Air Mobility (UAM). UAM requires vehicles capable of operations in the complex airspace of an urban environment. The National Aeronautics and Space Administration (NASA) is investigating representative vehicle configurations under the Revolutionary Vertical Lift Technology (RVLT) project. RVLT advances technologies that will increase speed, range, payload, and safety, and decrease noise, weight, emissions, and fuel burn. Currently, system designers associated with the project are concerned with vehicle component sizing using steady state vehicle models developed with the NASA Design and Analysis of Rotorcraft (NDARC) software [1,2]. NDARC is a numerical rotorcraft sizing and analysis tool that calculates performance and sizing metrics based on a full flight cycle by converging at notable steady state flight conditions such as idle, hover, and cruise [3]. Figure 1 shows a general mission profile for a UAM vehicle [4]. The mission profile was used with steady state NDARC vehicle simulations for sizing and analyses. The lack of sufficiently detailed information about transition between flight modes necessitates that the generic sizing mission contain a segment at maximum power for transitioning the aircraft [4]. However, investigations into the transient behavior of the UAM concept vehicle powertrains during transitions, which occur at the corner points of the curve in Figure 1, cannot be conducted using a steady state model. Furthermore, dynamic models are essential for the design and analysis of EAP system controllers. The behavior of UAM powertrains during transitions between notable flight conditions, and the need to develop controllers to regulate the EAP system during transitions, motivates the dynamic modeling effort presented in this paper. This effort aims to capture the interaction between multi-domain powertrain components to enable further system analysis and component sizing during flight condition transitions, as well as facilitate EAP control design. Any system analysis or sizing pertaining to transitions is out of the scope of this paper. This paper solely presents a dynamic model of the Side-By-Side (SBS) Hybrid UAM concept vehicle powertrain and outlines its fidelity and capabilities. Additional system analysis, both steady state and dynamic, will need to occur to accurately size each subsystem.

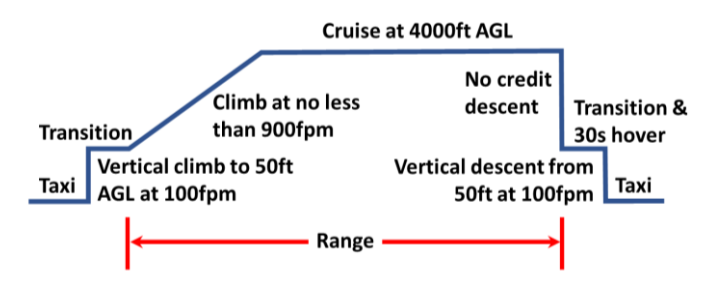


Figure 1. UAM FLIGHT MISSION PROFILE

This paper is organized as follows. Section 2 outlines the vehicle performance parameters and introduces the powertrain architecture. Section 3 describes the powertrain modeling component by component. Section 4 provides descriptions of the controllers used in the model. Section 5 presents results that highlight the operation of the model and its capabilities. Section 6 provides some concluding remarks and future work.

### 2. VEHICLE OVERVIEW

The SBS Hybrid UAM concept vehicle, shown in Figure 2, is a six passenger, dual rotor helicopter defined and actively investigated by the RVLT project [5]. System designers currently envision the SBS Hybrid as having a range of 200 nautical miles, comprising four 50 nautical mile trips, a maximum payload of 1200 pounds, and a cruising speed of 115 knots for the design mission profile. Shown in Figure 3 is a high-level graphical depiction of the SBS Hybrid powertrain. Two 187 hp turboshaft engines containing free power turbines drive the dual, overlapping rotors. The rotors each have a radius of 11.82 ft and a tip speed of 550 ft/sec. They are intermeshed and overlapped such that the hub-to-hub distance is 85% of the rotor diameter. Two independent freewheeling clutches connect the power turbines to a step down gearbox. A brake, which is used to bring the rotor to a stop quickly, is positioned between each rotor and its respective gearbox. Connected to the middle gearbox is a 100 hp electric machine (EM). An inverter connects a battery to the EM. The EM is used as a motor for hover and low speed flight, and as a generator in cruise to charge the battery. The battery is sized for 10 min (five 2-min segments) hover. The baseline aircraft uses an interconnect shaft for power distribution and control in the event of engine and/or motor failure [2,6]. This EAP architecture, in which the motor and engines are directly connected to the drivetrain, is known as parallel hybrid.

### 3. POWERTRAIN MODEL

The dynamic powertrain model is a hybrid model consisting of both analytical and numerical calculations constructed in the MATLAB  $^{\!(\!R\!)}/Simulink^{\!(\!R\!)}$  environment. The model is simulated at a time step of 20 milliseconds. Figure 4 is a schematic of the

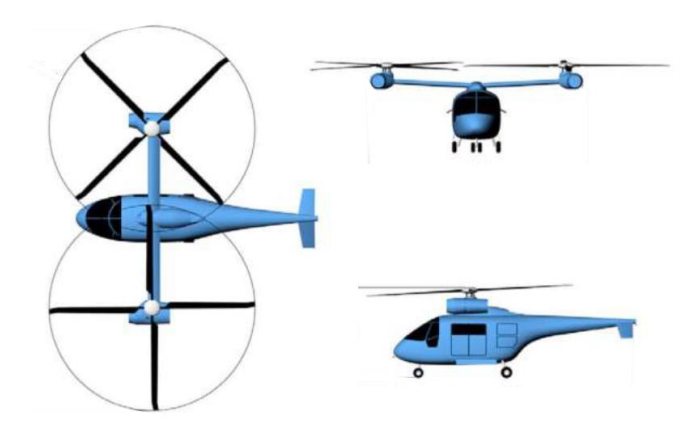


Figure 2. SIDE-BY-SIDE (SBS) HYBRID CONCEPT VEHICLE

2

This material is declared a work of the U.S. Government and is not subject to copyright protection in the United States. Approved for public release; distribution is unlimited.

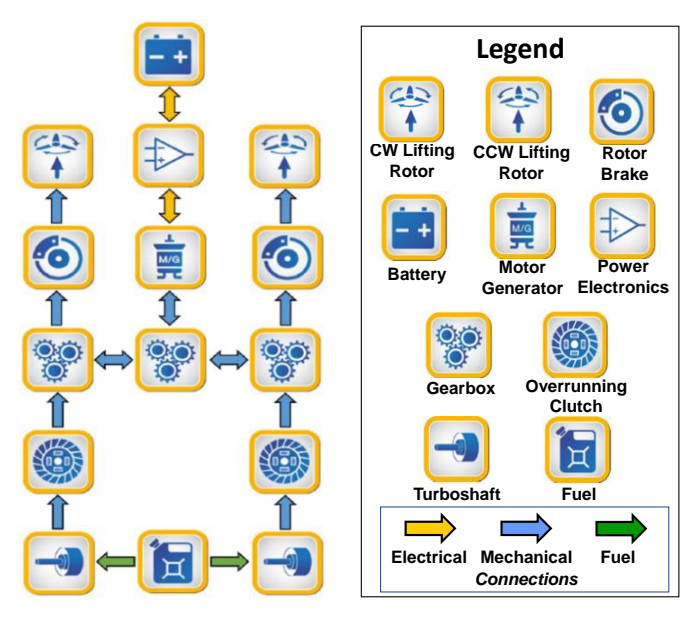


Figure 3. SIDE-BY-SIDE HYBRID POWERTRAIN CONCEPTUAL SCHEMATIC

powertrain model. Notable differences from Figure 3 to Figure 4 include the addition of the Power Turbine Shaft 1, Power Turbine Shaft 2, and Intermediate Shaft blocks, consolidation of electrical components into the Electrical Power System block, and the elimination of the Rotor Brake blocks. The addition of shaft blocks is necessary for modeling the dynamics associated with the mechanical system. Rotorcraft rotor brakes are used primarily for slowing down the rotor during vehicle shutdown and are thus not relevant to the current effort, so they were not included in the model. The following sections provide an explanation of the various subsystems within the model. Section 3.1 elaborates on the turboshaft engine models. Section 3.2 details the Mechanical Power Transmission System as well as its subsystems and calculations. Section 3.3 describes the electrical power system. Section 3.4 explains the rotor models. Refer to Figure 4 when reading the subsequent sections for a better understanding of the interaction between the powertrain components.

# 3.1 Turboshaft Engine

The powertrain contains two identical turboshaft engine models. The engines are modeled using the Toolbox for the Modeling and Analysis of Thermodynamic Systems (T-MATS) [7,8]. T-MATS is a NASA-developed library of Simulink® blocks that simplify the dynamic modeling, control design, and analysis of gas turbine engines. The T-MATS models were generated [9] directly from a 0-D model created using the Numerical Propulsion System Simulation (NPSS®) software [10], which is used for cycle design. Shaft inertia estimates are calculated based on models developed using the Weight

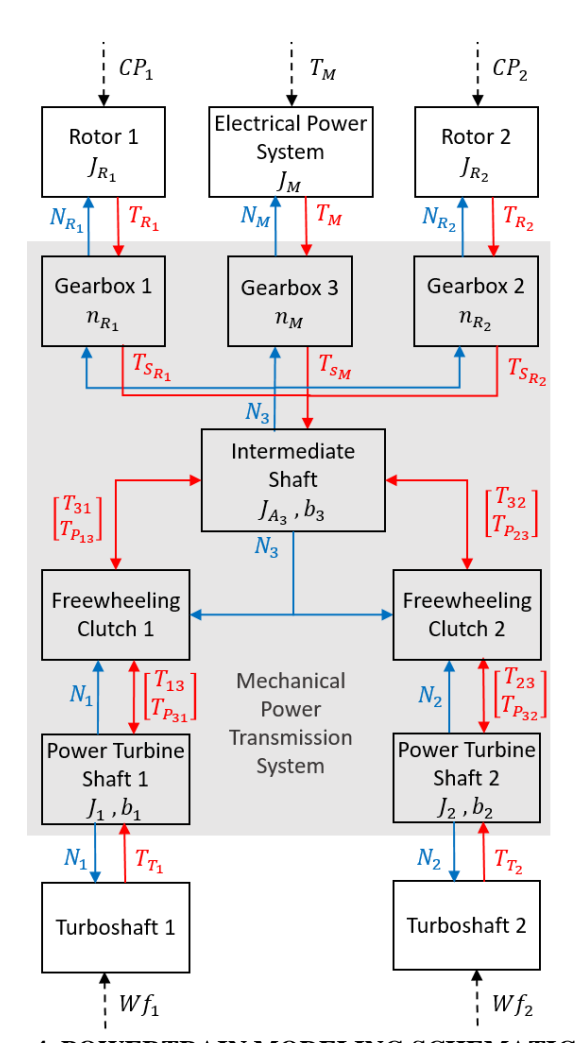


Figure 4. POWERTRAIN MODELING SCHEMATIC

Analysis of Turbine Engines (WATE++) software [11].\* Shown in Figure 5 is a graphical representation of the model construction. The single-spool engine model contains a gas generator consisting of a centrifugal compressor, burner, and high-pressure turbine, with the compressor and turbine mechanically connected by a shaft. The flow into the inlet is split between the compressor and bypass nozzle. The bypass nozzle rejects foreign objects and is a common feature on gas turbine engines that power rotorcraft. The compressor energizes the flow for combustion in the burner. The burner expels hot gas through the turbine to power the compressor. Cooling bleeds are extracted from the compressor to cool the turbine blades. The hot gas exits the turbine and passes through a power turbine aft of the gas generator. The power turbine shaft spins freely from the gas generator and is connected to the Mechanical Power Transmission System. The core nozzle expels hot gas from the engine but provides little thrust due to the large amount of work extracted from the flow by the power turbine. Engine size and estimated polytrophic efficiency curves define the design

<sup>\*</sup>Weight Analysis of Turbine Engine (WATE++) is an Object-Oriented computer code for gas turbine engine weight estimation that calculates the weight and dimension of each major gas turbine engine component.

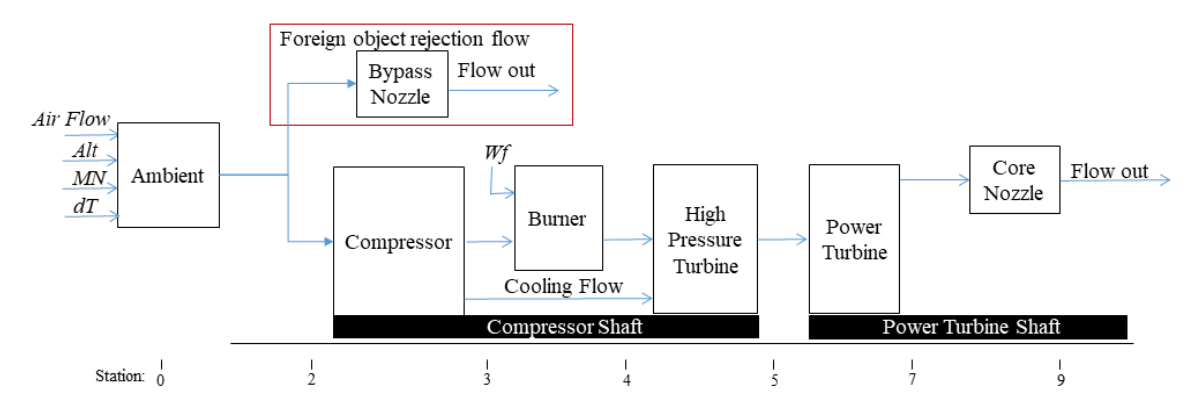


Figure 5. TURBOSHAFT ENGINE ARCHITECTURE

parameters of the engine. The maximum mechanical power produced per engine is 187 hp. A proportional-integral (PI) controller with integral windup protection (IWP) maintains the power turbine speed by regulating the fuel flow rate to the burner.

# 3.2 Mechanical Power Transmission System

The Mechanical Power Transmission System consists of multiple shafts, gearboxes, and freewheeling clutches that connect the power generating (e.g., turboshaft engines) and consuming (e.g., rotors) components of the powertrain model. The electrical power system is capable of both generating and consuming power. The following sections describe the models of each subsystem. Section 3.2.1 details the shaft models. Section 3.2.2 explains the freewheeling clutch models. Section 3.2.3 discusses the gearbox models.

# 3.2.1 Mechanical Shafts

The Power Turbine Shaft 1, Power Turbine Shaft 2, and Intermediate Shaft blocks in Figure 4 transmit mechanical power through the transmission system. Power Turbine 1 and 2 are considered the driving shafts while the Intermediate Shaft is the driven shaft. All three shafts spin at the same speed when the freewheeling clutches<sup>†</sup> are engaged, indicating that there is not a gearbox within the clutch model. Figure 6 shows the conventions used in the following shaft equations, the arrows indicate the positive direction for the variables. Equations (1), (2), (3), and (4) explain the operation of the Power Turbine Shaft 1 and Power Turbine Shaft 2 subsystems.

$$J_x \dot{N}_x - b_x N_x + T_{P_{3x}} + T_{T_x} = 0$$
(1)

$$\dot{N_x} = \begin{cases} \dot{N_x}, & N_x \le N_3 \ or \ \dot{N_x} < 0 \\ 0, & else \end{cases} \tag{2}$$

$$N_x = \min\left(\int \dot{N_x} dt, N_3\right) \tag{3}$$

$$T_{x3} = T_{T_x} - b_x N_x \tag{4}$$

Equations (5), (6), and (7) describe the operation of the Intermediate Shaft.

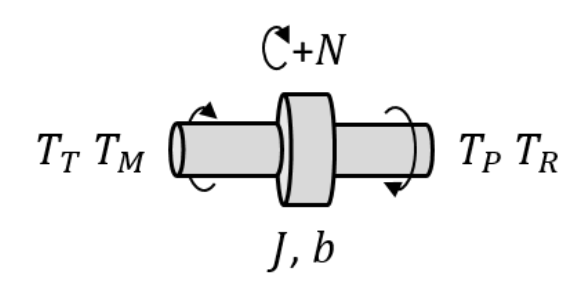


Figure 6. SHAFT VARIABLE CONVENTIONS

Angular moment of inertia, angular viscous damping, torque, angular speed, and angular acceleration are represented using the variables I, b, T, N, and  $\dot{N}$ , respectively. Pertaining to the previous variables, a subscript x represents either Power Turbine Shaft 1 or Power Turbine Shaft 2 with 1 and 2, respectively. The Intermediate Shaft is represented by subscript 3. The subscript T denotes the turboshaft. Subscript P denotes the variable after it is passed through the freewheeling clutch logic. Additional subscripts containing two numbers abide by the following convention: the first number denotes the source of the variable, the second number denotes the destination. For example,  $T_{P_{2,1}}$  is read as the torque from the Intermediate Shaft acting on Power Turbine Shaft 1 after having passed through an engaged Freewheeling Clutch 1. Additionally,  $T_{13}$  is read as the torque from Power Turbine Shaft 1 acting on the Intermediate Shaft if passed through Freewheeling Clutch 1. The min () function takes the minimum value of the two arguments. Equation (1) is the torque balance for the power turbine shafts. Equations (2) and (3) dynamically limit the speed of the power turbine shafts to not exceed the speed of the Intermediate Shaft. The previous logic captures the nonlinear behavior of the system due to the mechanical limit imposed by the freewheeling clutch.

<sup>&</sup>lt;sup>†</sup>A freewheeling or overrunning clutch is one that disengages the driving shaft from the driven shaft when the driven shaft's rotational speed is faster, preventing the transmission from spinning an inoperative engine.

$$J_3 \dot{N}_3 - b_3 N_3 + T_{P_{13}} + T_{P_{23}} + T_{S_{R_1}} + T_{S_{R_2}} + T_{S_M} = 0 \qquad (5)$$

$$T_{32} = T_{S_{R_1}} + T_{S_{R_2}} + T_{S_M} - b_2 N_2 + T_{P_{13}}$$
 (6)

$$T_{31} = T_{S_{R_1}} + T_{S_{R_2}} + T_{S_M} - b_3 N_3 + T_{P_{23}}$$
 (7)

Subscripts R and M denote the rotor and motor, respectively. Additional subscripts 1 and 2 after R specify Rotor 1 and Rotor 2, respectively. Equation (5) is the torque balance of the Intermediate Shaft. Equations (4), (6), and (7) calculate the torque passed from the source shaft to the clutch of the destination shaft. The next section describes additional logic that represents the nonlinear behavior of the freewheeling clutches.

#### 3.2.2 Freewheeling Clutch

Freewheeling Clutch 1 and 2 are mechanical power transmission devices that allow for unidirectional torque transmission across the clutch. For engagement to occur, the driver shaft speed must be equal to the driven side speed. The driver shaft is the input shaft. The driven shaft is the output shaft. When engaged, the driver shaft is mechanically coupled to the driven shaft, enabling it to transmit torque. The mechanical interaction through the clutch does not allow the driver shaft speed to exceed the driven shaft speed. When the driver shaft speed is less than the driven shaft speed, the clutch is disengaged. When disengaged, the driver shaft is not mechanically coupled to the driven shaft and spins independent of the driven shaft. In this case, torque cannot be transmitted through the clutch. Figure 7 shows the conventions used in the following equations. Equations (8) and (9) regulate the torque passed through the respective freewheeling clutches.

T<sub>P<sub>3y</sub></sub> = 
$$\begin{cases} T_{y3}, & N_y = N_3 \text{ and } T_{y3} > 0 \\ 0, & else \end{cases}$$

$$T_{P_{3y}} = \begin{cases} T_{3y}, & N_y = N_3 \text{ and } T_{3y} < 0 \\ 0, & else \end{cases}$$

$$(8)$$

$$T_{P_{3y}} = \begin{cases} T_{3y}, & N_y = N_3 \text{ and } T_{3y} < 0 \\ 0, & else \end{cases}$$

$$T_{P_{3y}} = \begin{cases} T_{3y}, & N_y = N_3 \text{ and } T_{3y} < 0\\ 0, & else \end{cases}$$
 (9)

The freewheeling clutch number is denoted by y. Equation (8) states that a positive torque on the driver side is transmitted through the clutch to the driven side when the speeds of both

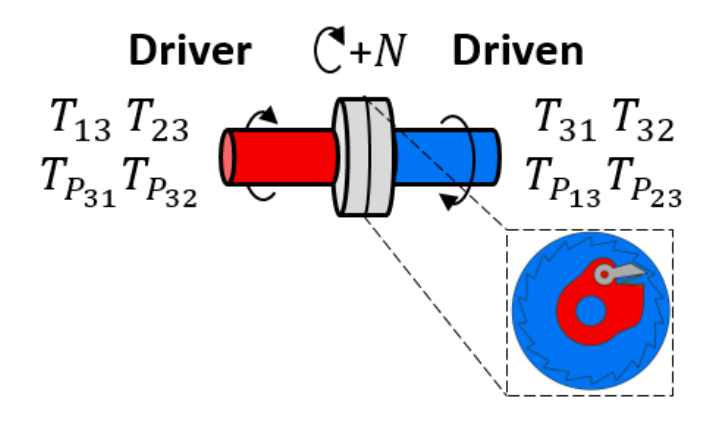


Figure 7. FREEWHEELING CLUTCH VARIABLE **CONVENTIONS** 

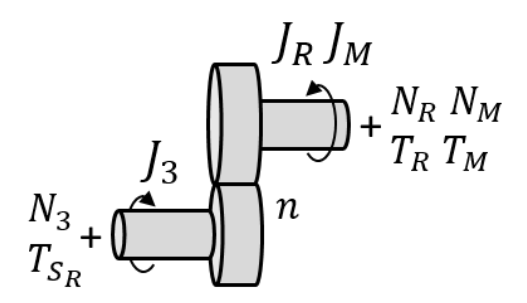


Figure 8. GEARBOX VARIABLE CONVENTIONS

sides are equal. Equation (9) states that a negative torque on the driven side is transmitted through the clutch to the driver side when the speeds of both sides are equal.

#### 3.2.3 **Gearbox**

Gearbox 1, 2, and, 3 are mechanical power transmission devices containing gear trains that step down the speed of the Intermediate Shaft to its respective coupled subsystems. Figure 8 depicts the gearbox conventions used. Gearbox 1 and 2 pass torque from the rotors to the Intermediate Shaft. Gearbox 3 passes torque between the Electrical Power System and the Intermediate Shaft. This statement implies that the Electrical Power System is capable of both extracting power from and transferring power to the Mechanical Power Transmission System. Equations (10), (11), (12), (13), (14), and (15) describe the operation of Gearboxes 1, 2, and 3.

$$N_{R_1} = \frac{1}{n_{R_2}} N_3 \tag{10}$$

$$T_{S_{R_1}} = \frac{\eta_{R_1}}{n_{R_1}} T_{R_1}$$

$$N_{R_2} = \frac{1}{n_{R_2}} N_3$$

$$T_{S_{R_2}} = \frac{\eta_{R_2}}{n_{R_2}} T_{R_2}$$

$$N_M = \frac{1}{n_M} N_3$$

$$\eta_M$$
(11)

$$N_{R_2} = \frac{1}{n_{R_2}} N_3 \tag{12}$$

$$T_{S_{R_2}} = \frac{\eta_{R_2}}{n_{R_2}} T_{R_2} \tag{13}$$

$$N_M = \frac{1}{n_M} N_3 \tag{14}$$

$$T_{S_M} = \frac{\eta_M}{n_M} T_M \tag{15}$$

The gear ratio and gearbox efficiency are represented by variables n and  $\eta$ , respectively. The gear ratio convention n > 1steps down the speed from the Intermediate Shaft to each respective coupled subsystem. Subscript S denotes the scaled value of the variable after augmentation by the gearbox. Equation (16) represents the augmented inertia of the Intermediate Shaft due to the reflection of the inertias through the three gearboxes. Gearbox reflection is the augmentation of the inertial (or viscous damping) load felt by the driving system due to the mechanical advantage of the gearbox.

$$J_{A_3} = J_3 + \frac{1}{n_{R_1}^2} J_{R_1} + \frac{1}{n_{R_2}^2} J_{R_2} + \frac{1}{n_M^2} J_M$$
 (16)

Subscript A denotes the augmented variable due to the mechanical advantage of the gearbox. In this powertrain, the mechanical advantage of the gearboxes reduces the inertial load

This material is declared a work of the U.S. Government and is not subject to copyright protection in the United States. Approved for public release; distribution is unlimited.

felt by the Intermediate Shaft from Rotor 1, Rotor 2, and the Electrical Power System.

# 3.3 Electrical Power System

The Electrical Power System consists of an EM, an inverter, and a supercapacitor<sup>‡</sup> in series. The EM is mechanically coupled to Gearbox 3 of the Mechanical Power Transmission System and is capable of operating in either generator mode (power extraction) or motor mode (power insertion). The inverter electrically couples the EM to the supercapacitor. The inverter modulates the voltage and current given to the EM during operation and is capable of bi-directional power flow. Both the EM and inverter are modeled using power balance equations that contain efficiency losses. Each component efficiency loss is calculated via a user defined efficiency map. The supercapacitor is electrically coupled to the inverter and is modeled using physics-based equations as a series resistive-capacitive circuit. The supercapacitor is capable of both supplying and absorbing power. The Electrical Power System is modeled using the Electrical Modeling and Thermal Analysis Toolbox (EMTAT) [12,13]. EMTAT is a NASA-developed library of Simulink® blocks that simplify the modeling of electrical power systems for EAP applications and is a complementary toolbox to T-MATS. The Electrical Power System augments the engines during low speed flight and hover; it charges the energy storage device during cruise.

### 3.4 Rotors

Rotor 1 and 2 are mechanically coupled to Gearbox 1 and 2, respectively. The rotors produce the required thrust for the vehicle during flight. The thrust is calculated using empirical methods and aerodynamic theory. The torque needed to produce the required thrust is calculated using blade element theory. All calculations are based on a numerical rotor model developed using the approach in the NDARC software. A Newton-Raphson iterative solver, found in both the T-MATS and EMTAT libraries, is used to drive the system of equations to convergence. The rotors operate at a fixed speed. Thrust is modulated by changing the collective pitch, *CP*, of the rotor blades. Currently, the rotors approximate the torque needed to produce the required thrust. A comprehensive sizing of the rotor model is out of the scope of this paper. The rotor model is sized sufficiently to display the conceptual operation of the powertrain.

# 4. CONTROLLERS

The SBS Hybrid powertrain utilizes controllers to regulate the interaction between the components of the multi-domain powertrain. The inner loop of the control system consists of the individual turboshaft fuel flow rate controllers. The controllers regulate the speed of the power turbine using PI controllers with IWP. The outer loop, denoted as the torque-sharing controller, balances the torque produced by each power turbine while ensuring the speed setpoint is reached at steady state. Figure 9 is

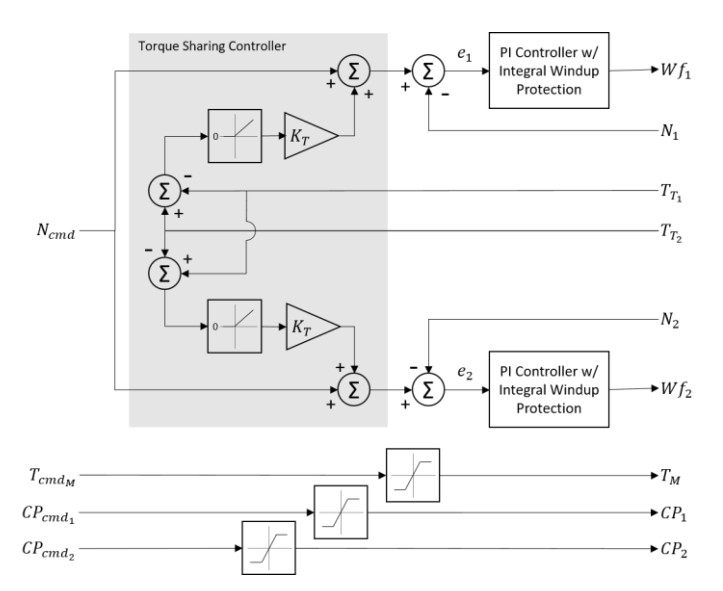


Figure 9. CONTROLLER MODELING DIAGRAM

a block diagram representation of the SBS Hybrid propulsion control system. Commanded variables include the power turbine speed command, the EM torque command, and the collective pitch command of Rotors 1 and 2, denoted  $N_{cmd}$ ,  $T_{cmd_M}$ ,  $CP_{cmd_1}$ , and  $CP_{cmd_2}$ , respectively. Control inputs to the system are the Turboshaft 1 and 2 fuel flow rate demanded by the controller, the collective pitch of Rotor 1 and 2, and the EM torque, denoted  $Wf_1$ ,  $Wf_2$ ,  $CP_1$ ,  $CP_2$ , and  $T_M$ , respectively. The measured (feedback) variables used by the controller are the speeds of Power Turbine Shaft 1 and 2 as well as the torque produced by the power turbines of Turboshaft 1 and 2, denoted  $N_1$ ,  $N_2$ ,  $T_{T_1}$ , and  $T_{T_2}$ , respectively. Variables  $e_1$  and  $e_2$  represent the speed error into the fuel flow rate controllers.  $K_T$  is the gain of the torque-sharing controller. As  $K_T$  increases, the convergence time of the power turbine torques decreases.

The torque-sharing controller balances the torque produced by the power turbines of Turboshafts 1 and 2 while maintaining their desired nominal speed [14]. It works by creating an artificial speed setpoint increase as a means to increase the power of the lower producing engine until the torques match. Without this artifice, the two engines can rotate at the same speed but not support the load equally. The torque-sharing controller continually calculates a speed setpoint bias, which is applied to the turboshaft engine producing the lesser torque, as shown in the shaded portion of Figure 9. It computes the setpoint bias by subtracting the lesser of the measured power turbine torques from the greater and multiplying this difference by a positive gain,  $K_T$ ; thus, the bias is proportional to the torque difference. The controller of the lower producing engine reacts by increasing the fuel flow rate. As that engine provides more torque, offsetting more of the load, the higher producing engine's controller decreases its fuel flow rate to maintain its speed setpoint. As the two engines' measured torques converge, the bias decreases. The

<sup>&</sup>lt;sup>‡</sup>For this model the developers arbitrarily chose to use the EMTAT supercapacitor component rather than a battery component.

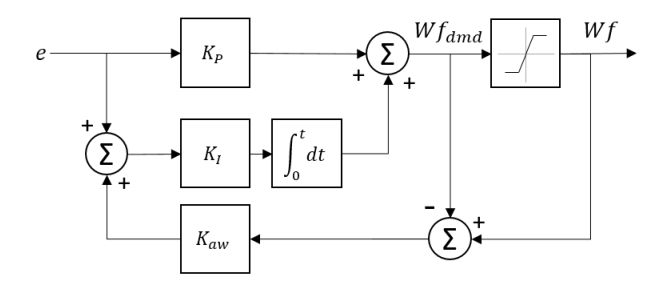


Figure 10. PI CONTROLLER WITH IWP MODELING DIAGRAM

torques converge more quickly with larger values of  $K_T$ . This "match the maximum" torque sharing approach prevents the situation in which a good engine is commanded to reduce power to match a power-limited engine [14].

Both turboshaft engines utilize PI setpoint controllers to regulate the speed of the power turbine (Figure 10). The proportional and integral gains are denoted by  $K_P$  and  $K_I$ , respectively. In practice, engine controllers maintain a variety of operational limits (e.g., acceleration, deceleration) and safety limits (e.g., gas generator speed, temperature) [15]. Adherence to these limits has the potential to impact engine responsiveness, and in extreme cases may prevent the engine from achieving its setpoint. In these cases, the integral of the error signal continuously increases, or "winds up," which causes a delayed response to a setpoint change while the control signal "unwinds" and comes off its limit. IWP protects against this by driving the fuel flow demand toward the active limit, enabling a rapid response to a setpoint change. In the limited case, the logic in Figure 10 calculates a turboshaft fuel flow rate demand,  $Wf_{dmd}$ , that approximates the saturation limit of the fuel flow rate. The anti-windup gain,  $K_{aw}$ , can be tuned to vary the magnitude of the error correction.

# 5. RESULTS AND DISCUSSION

Six simulations show responses to setpoint changes, controller activations, and limiting conditions. The following list describes the various simulations:

- 1. Power Turbine Speed Setpoint Change
- 2. Rotor Collective Pitch Setpoint Change
- 3. Motor Torque Setpoint Change
- 4. Activation of Torque Sharing Controller
- 5. Clutch Disengagement Situation
- Fuel Flow Limited by IWP Logic

All simulations occur at sea-level static standard day conditions (Alt = 0 ft, MN = 0, and 59 °F) and begin at a steady state condition. Each simulation changes only one input variable type that affects the response of the system.

Figure 11 shows responses to increasing and decreasing step changes in the power turbine shaft speed setpoint of both engines simultaneously. The plotted variables are (top) the two Power Turbine Shaft speeds ( $N_1$  and  $N_2$ ), the Intermediate Shaft speed ( $N_3$ ), and commanded speed ( $N_{cmd}$ ); (middle) the Turboshaft 1 and 2 fuel flow rates ( $Wf_1$  and  $Wf_2$ ); and (bottom) Turboshaft 1

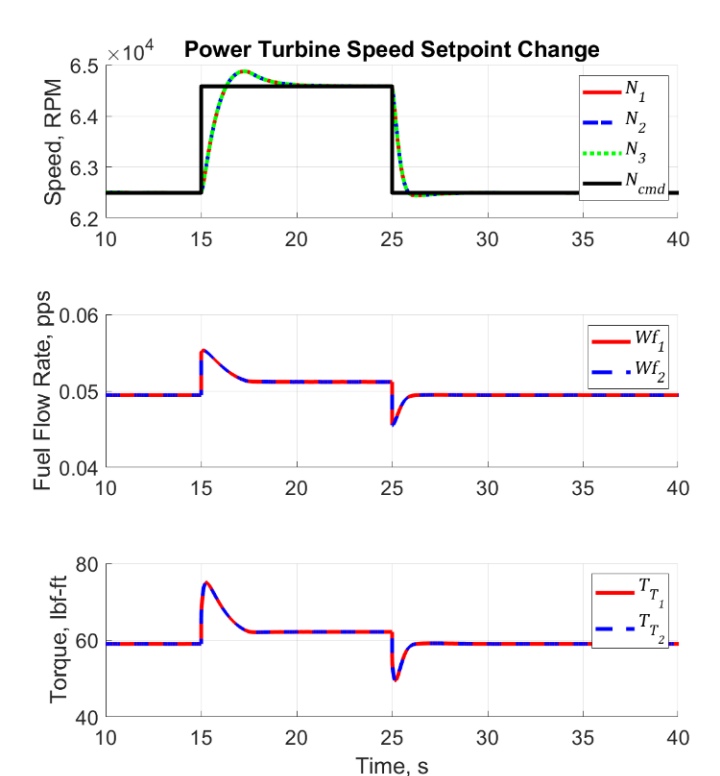


Figure 11. RESPONSE TO A POWER TURBINE SPEED SETPOINT CHANGE

and 2 power turbine torque ( $T_{T_1}$  and  $T_{T_2}$ ). The plots show slightly underdamped yet nominal response to speed setpoint step changes. Note that the power turbines are intended to operate at a constant speed. This small (3%) speed change simulation is for demonstration only.

Figure 12 shows the responses to increasing and decreasing step changes in the collective pitch angle of the two rotors simultaneously. This corresponds to transition from hover to climb or climb to cruise. The plotted variables are (top) Rotor 1 and 2 collective pitch angles  $(CP_1 \text{ and } CP_2)$ ; (second from top) the two Power Turbine Shaft speeds  $(N_1 \text{ and } N_2)$ , the Intermediate Shaft speed  $(N_3)$ , and commanded speed  $(N_{cmd})$ ; (third from top) the Turboshaft 1 and 2 fuel flow rates ( $Wf_1$  and  $Wf_2$ ); and (bottom) Turboshaft 1 and 2 power turbine torque ( $T_{T_1}$ and  $T_{T_2}$ ). The plots show a nominal response to the load change on the turboshaft engines brought about by the change in the collective pitch angle. The fuel flow rate of both engines adjusts to supply the required amount of torque to drive the shaft speeds to their setpoints. Overshoot is present in both the fuel flow rate and power turbine torque plots. Refining the PI speed controller gains will eliminate overshoot in the response.

Figure 13 shows the responses to step changes in the motor torque setpoint. This corresponds roughly to the transition from cruise to hover toward the end of the mission, when the EM switches from charging the supercapacitor to augmenting the engine power. The plotted variables are (top) the two Power Turbine Shaft speeds ( $N_1$  and  $N_2$ ), the Intermediate Shaft speed

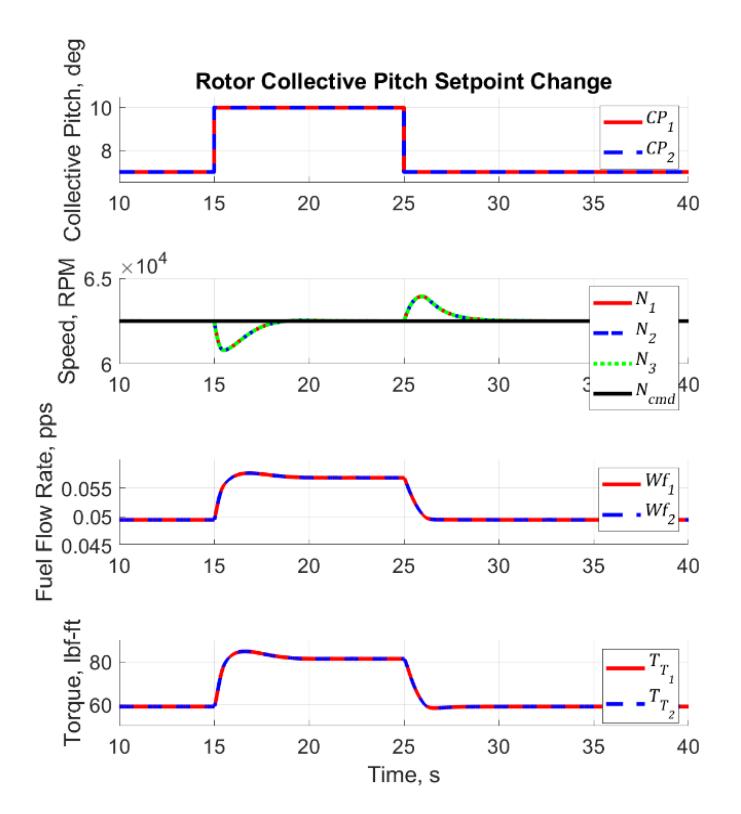


Figure 12. RESPONSE TO A ROTOR COLLECTIVE PITCH SETPOINT CHANGE

 $(N_3)$ , and commanded speed  $(N_{cmd})$ ; (second from top) the Turboshaft 1 and 2 fuel flow rates  $(Wf_1 \text{ and } Wf_2)$ ; (third from top) Turboshaft 1 and 2 power turbine torque  $(T_{T_1} \text{ and } T_{T_2})$  and the EM torque  $(T_M)$ ; and (bottom) supercapacitor state of charge. A positive motor torque applies power to the Mechanical Power Transmission System. A negative torque extracts power from the Mechanical Power Transmission System. The plots show nominal responses to load increases and decreases on the system by the EM as well as proper charging and discharging of the supercapacitor during power insertion and extraction.

Figure 14 demonstrates the torque-sharing controller. The plotted variables are (top) the flag indicating activation of torque sharing; (second from top) the two Power Turbine Shaft speeds  $(N_1 \text{ and } N_2)$ , the Intermediate Shaft speed  $(N_3)$ , and commanded speed including biases ( $N_{cmd+bias_1}$  and  $N_{cmd+bias_2}$ ); (third from top) the Turboshaft 1 and 2 fuel flow rates (Wf<sub>1</sub> and Wf<sub>2</sub>); and (bottom) Turboshaft 1 and 2 power turbine torque ( $T_{T_1}$  and  $T_{T_2}$ ).  $N_{cmd+bias_1}$  and  $N_{cmd+bias_2}$  are the augmented power turbine speed setpoints of Turboshafts 1 and 2. They consist of the power turbine speed setpoint plus a speed command bias calculated by the torque-sharing controller. Initially, Turboshaft 2 is supporting less of the powertrain load. Upon enabling of the torque-sharing controller algorithm, the positive torque error between the two engines causes a bias to be applied to the original speed setpoint of Turboshaft 2. The increased speed setpoint causes an increase in the fuel flow rate to Turboshaft 2, which results in increased torque production by the power

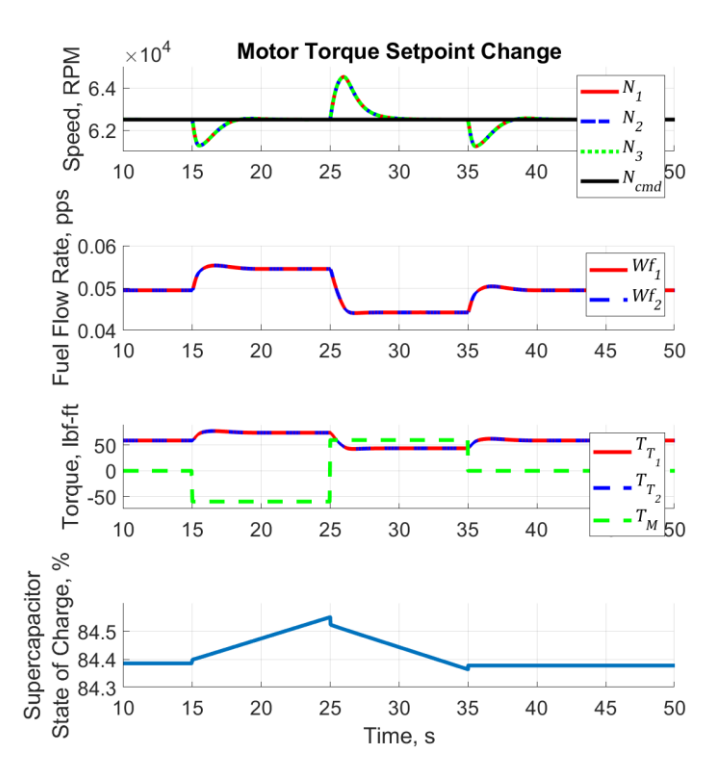


Figure 13. RESPONSE TO A MOTOR TORQUE SETPOINT CHANGE

turbine. As the torque of Turboshaft 2 increases, it begins to support a larger portion of the load. Turboshaft 1 reacts to the decrease in supported load by lowering its power turbine torque production to avoid accelerating. Once the torques become equal, the bias on the Turboshaft 2 speed setpoint returns to zero. It is important to note that the fuel flow rates converge to the same value because the turboshaft engine models are identical.

Figure 15 shows a situation where Clutch 2 is purposely disengaged due to a decrease in the commanded power turbine speed of Turboshaft 2. Torque sharing is turned off in this case. The variables shown are (top) the Power Turbine Shaft speeds  $(N_1 \text{ and } N_2)$ , the Intermediate Shaft speed  $(N_3)$ , and the individual power turbine speed commands ( $N_{cmd_1}$  and  $N_{cmd_2}$ ); (second from top) Turboshaft 1 and 2 fuel flow rates ( $Wf_1$  and  $Wf_2$ ); (third from top) Turboshaft 1 and 2 power turbine torques ( $T_{T_1}$  and  $T_{T_2}$ ); and (bottom) the percent of the load supported by both turboshaft engines together. The disengagement of Turboshaft 2 from the rest of the powertrain occurs due to a power turbine speed setpoint decrease to a lower magnitude than the power turbine speed setpoint of Turboshaft 1, causing a reduction in both the fuel flow rate and torque produced by Power Turbine 2. As the power turbine torque of Turboshaft 2 decreases, the power turbine torque of Turboshaft 1 increases to maintain its speed setpoint while supporting the powertrain load. The bottom graph of Figure 15 plots the percentage of the load supported by both power turbines together. When less than 100, the Intermediate Shaft and Power Turbine Shaft 2 decelerate. When greater than 100, the shafts accelerate. The immediate decrease in load supported at 20 seconds (and the decrease in the shaft speeds) is

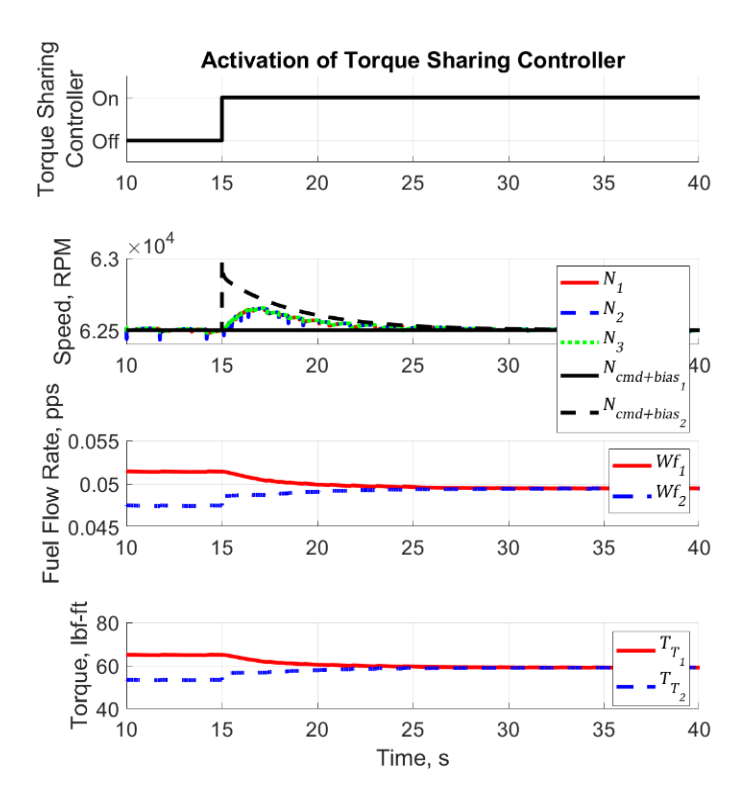


Figure 14. RESPONSE TO THE ACTIVATION OF THE TORQUE SHARING CONTROLLER

due to a non-symmetric change between the torque produced by the power turbines of the two turboshaft engines. More specifically, the power turbine torque of Turboshaft 2 is decreasing more quickly than the torque of Turboshaft 1 is increasing. Only at 24 seconds does the power turbine of Turboshaft 1 produce enough torque to hold the entire powertrain load. At that point, Turboshaft 2 disengages from the powertrain and Turboshaft 1 proceeds to regulate its power turbine speed to its desired setpoint. Note that in an actual implementation there may not be sufficient power available to achieve the setpoint in all cases [2].

The quick speed decrease of Turboshaft 2 following clutch disengagement is due to an abnormally high viscous damping value specified for the power turbine shaft. The T-MATS Turbine block limits the torque produced by the power turbine. The lower limit occurs when the T-MATS Iterative Newton-Raphson Solver does not converge. In order to slow the speed of the Power Turbine Shaft 2 during a clutch disengagement situation, the shaft must have a load torque due to vicious damping that is greater than this limit. While the behavior of the disengaged power turbine itself may not be realistic, it has no impact to the rest of the powertrain simulation. As the vehicle design is refined, the model parameters and/or T-MATS library blocks can be updated to better reflect the behavior of the powertrain during all modes of operation.

As an aside, the subtle notches in the speed plots of Figure 14 and Figure 15 are due to the sensitivity of the logic that determines clutch engagement. As long as the driver side shaft speed of the clutch exactly equals the driven side speed ( $N_1$  =

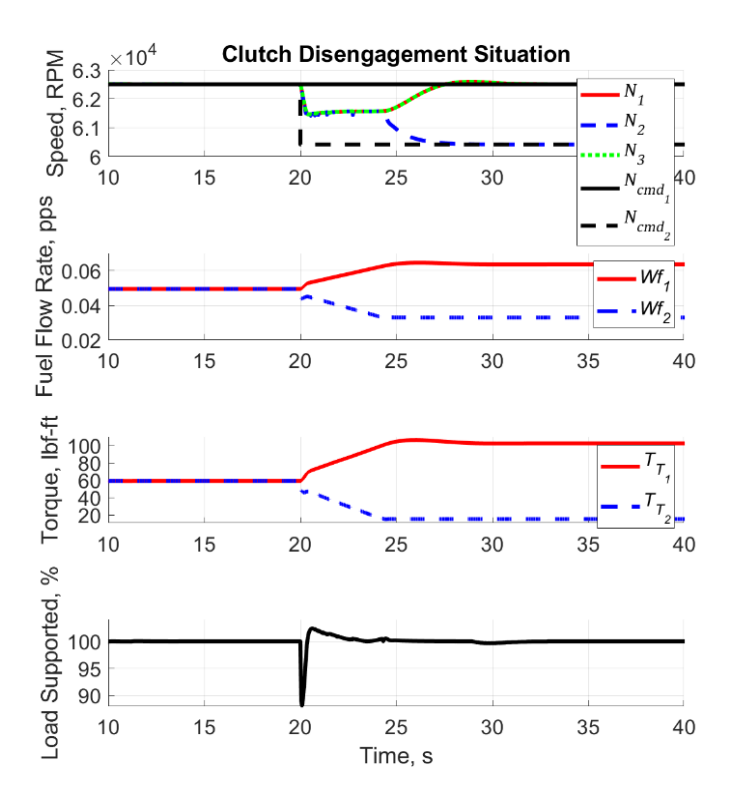


Figure 15. CLUTCH DISENGAGEMENT SITUATION

 $N_3$  or  $N_2 = N_3$ ), the respective clutch is engaged. Due to the numerical computations related to the interaction of the model components, occasionally a power turbine speed may appear to drop slightly below that of the Intermediate Shaft, and the clutch briefly disengages, resulting in a notch on the speed plot. The reengagement may require several time steps to complete as the simulation progresses. The addition of a small dead zone in the clutch logic might alleviate this issue.

Figure 16 demonstrates the IWP logic. Here a simultaneous rotor collective pitch setpoint change forces the fuel flow rate to hit a pre-determined limit. This causes the power turbine speed to drop, creating a steady state error. The plotted variables are (top) collective pitch angle of the two rotors  $(CP_1 \text{ and } CP_2)$ ; (second from top) Power Turbine Shaft speeds ( $N_1$  and  $N_2$ ), the Intermediate Shaft speed  $(N_3)$ , and the individual power turbine speed commands ( $N_{cmd_1}$  and  $N_{cmd_2}$ ); (third from top) Turboshaft 1 and 2 fuel flow rates ( $Wf_1$  and  $Wf_2$ ), along with the limit and computed demand ( $Wf_{dmd}$ ); and (bottom) Turboshaft 1 and 2 power turbine torque  $(T_{T_1}$  and  $T_{T_2})$ . The limit value is arbitrarily chosen to show the performance of the IWP logic. The fuel flow rate demand,  $Wf_{dmd}$ , is calculated by the power turbine PI speed controller. In this scenario, the fuel flow rate demand is the same for both engines. As the fuel flow rate saturates, the IWP logic drives  $W f_{dmd}$  to the fuel flow rate limit rather than letting it grow unabated. When the collective pitch setpoint is decreased, the fuel flow demand immediately moves off the limit, avoiding the delay associated with integrator windup during saturation.

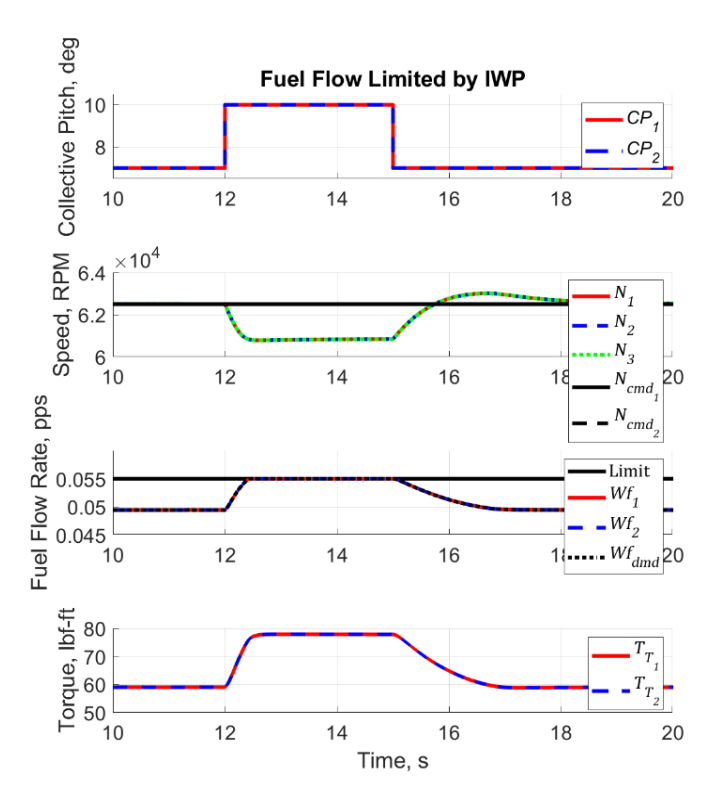


Figure 16. RESPONSE TO THE ACTIVATION OF THE INTEGRAL WINDUP PROTECTION LOGIC

### **REFERENCES**

- [1] Silva, Christopher, Johnson, Wayne, Antcliff, Kevin, and Patterson, Michael. "VTOL Urban Air Mobility Concept Vehicles for Technology Development." Aviation Technology, Integration, and Operations Conference. AIAA 2018-3847. Atlanta, GA, June 25-29, 2018.
- [2] Johnson, Wayne, Silva, Christopher, and Solis, Eduardo. "Concept Vehicles for VTOL Air Taxi Operations." AHS International Technical Meeting Aeromechanics Design for Transformative Vehicle Flight. San Francisco, CA, January 16-19, 2018.
- [3] Johnson, Wayne, "NDARC NASA Design and Analysis of Rotorcraft." NASA/TP-2015-218751. April 2015.
- [4] Patterson, Michael D., Antcliff, Kevin R., and Kohlman, Lee W. "A Proposed Approach to Studying Urban Air Mobility Missions Including an Initial Exploration of Mission Requirements." American Helicopter Society 74th Annual Forum, Phoenix, AZ, May 14-17, 2018.
- [5] Ventura Diaz, Patricia, Johnson, Wayne, Ahmad, Jasmin, and Yoon, Seokkwan. "The Side-by-Side Urban Air Taxi Vehicle." AIAA Aviation Forum. AIAA 2019-2828. Dallas, TX, June 17-21, 2019.
- [6] Darmstadt, Patrick R., Catanese, Ralph, Beiderman, Allan, Dones, Fernando, Chen, Ephraim, Mistry, Mihir P., Babie,

### 6. CONCLUSION

The dynamic powertrain model for the Side-By-Side (SBS) Hybrid concept aircraft presented in this paper simulates the concept of operation and the dynamics of the multi-domain system. Estimated subsystem parameters were used that capture the powertrain operation during transients. Results pertaining to the perturbation of individual system inputs display the model features and associated responses, which are representative of behaviors that occur during flight mode transitions. Integration with a vehicle model would enable more meaningful simulations of the full flight profile. Future work includes obtaining more precise subsystem parameters from system-level design studies of the vehicle. This could also include modifying the turboshaft engine model to enable more realistic behavior when the engine is disconnected from the load. This work will enable the analysis of the vehicle response characteristics during flight mode transitions, provide a platform to design an effective control system for the hybrid-electric vehicle, and provide a testbed for optimizing the coordination of the motor and gas turbine engines over the flight profile.

### **ACKNOWLEDGMENTS**

The authors wish to acknowledge Julian Hernandez and T. Shane Sowers for their guidance on Simulink® powertrain modeling and Chris Snyder for consultation on subsystem level parameter specifications. The authors also thank the Transformative Aeronautics Concepts Program (TACP)/Transformational Tools and Technologies (TTT) project, and the Arizona Space Grant Consortium for supporting this work.

- Brian, Beckman, Mary, and Preator, Robin. "Hazards Analysis and Failure Modes and Effects Criticality Analysis (FMECA) of Four Concept Vehicle Propulsion Systems." NASA/CR—2019-220217. June 2019.
- [7] Chapman, Jeffryes W., Lavelle, Thomas M., May, Ryan D., Litt, Jonathan S., and Guo, Ten-Huei. "Toolbox for the Modeling and Analysis of Thermodynamic Systems (T-MATS) User's Guide." NASA/TM—2014-216638. January 2014.
- [8] Chapman, Jeffryes W., Lavelle, Thomas M., May, Ryan D., Litt, Jonathan S., and Guo, Ten-Huei. "Propulsion System Simulation Using the Toolbox for the Modeling and Analysis of Thermodynamic Systems (T-MATS)." AIAA Propulsion and Energy Forum. AIAA 2014-3929. Cleveland, OH, July 28-30, 2014.
- [9] Chapman, Jeffryes W., Lavelle, Thomas M., Litt, Jonathan S., and Guo, Ten-Huei. "A Process for the Creation of T-MATS Propulsion System Models from NPSS Data." AIAA 2014-3931, 50th AIAA/ASME/SAE/ASEE Joint Propulsion Conference, Cleveland, OH, July 28-30, 2014.
- [10] Jones, S.M. "Steady-State Modeling of Gas Turbine Engines Using the Numerical Propulsion System

- Simulation Code." *ASME Turbo Expo 2010: Power for Land, Sea, and Air.* GT2010-22350, Glasgow, UK, June 14–18, 2010.
- [11] Tong, Michael T., and Naylor, Bret A. "An Object-Oriented Computer Code for Aircraft Engine Weight Estimation." ASME Turbo Expo 2008: Power for Land, Sea, and Air. GT2008-50062, Berlin, Germany, June 9–13, 2008
- [12] Bell, Mark E., and Litt, Jonathan S. "Electrical Modeling and Thermal Analysis Toolbox (EMTAT) User's Guide." NASA/TM-20205008125. October 2020.
- [13] Bell, Mark E., and Litt, Jonathan S. "An Electrical Modeling and Thermal Analysis Toolbox for Electrified

- Aircraft Propulsion Simulation." *AIAA Propulsion and Energy Forum.* AIAA 2020-3676. August 24-28, 2020.
- [14] Chiuchiolo, E. A., and Curran, J. J. "Three-Engine Control System for the Prototype EH-101 Helicopter." Seventh European Rotorcraft and Powered Lift Forum, Paper No. 18. Garmisch-Partenkirchen, Germany, September 8-11, 1981
- [15] Curran. J.J. "T700 Fuel and Control System—A Modern System Today for Tomorrow's Helicopters." 29th Annual National Forum of the American Helicopter Society. Preprint No. 771. Washington, D.C., May 1973.